Circular rogue wave clusters

David J. Kedziora,* Adrian Ankiewicz, and Nail Akhmediev
Optical Sciences Group, Research School of Physics and Engineering, The Australian National University, Canberra ACT 0200, Australia
(Received 28 July 2011; published 28 November 2011)

Using the Darboux transformation technique and numerical simulations, we study the hierarchy of rational solutions of the nonlinear Schrödinger equation that can be considered as higher order rogue waves in this model. This analysis reveals the existence of rogue wave clusters with a high level of symmetry in the (x,t) plane. These structures arise naturally when the shifts in the Darboux scheme are taken to be eigenvalue dependent. We have found single-shell structures where a central higher order rogue wave is surrounded by a ring of first order peaks on the (x,t) plane.

DOI: 10.1103/PhysRevE.84.056611 PACS number(s): 05.45.Yv, 47.20.Ky, 42.65.−k

I. INTRODUCTION

The notion of rogue waves first appeared in studies of deep ocean waves [1–3] and gradually moved to other fields of physics such as optics [4], capillary waves [5], superfluidity [6], Bose-Einstein condensates (BECs) [7], etc. There are various approaches in these studies, starting from linear wave analysis [8], which can explain some of the phenomena that involve high amplitudes. However, the most comprehensive approach is based on nonlinear physics [1].

In particular, deep ocean waves, as described by the nonlinear Schrödinger equation (NLSE) [1], have specific solutions which are localized in both space and time. Such localization is exemplified by the Peregrine soliton, which has been studied both theoretically [9,10] and experimentally [11,12]. There is now growing interest in identifying higher order rational solutions [13–19], which are also doubly localized. Recent publications by Matveev's group significantly developed the technique of obtaining multirogue wave solutions and presented explicit forms for these higher order structures [15,17–20]. However, the complexity of these solutions does not allow for easy manipulation, despite being provided in analytical form. Even plotting them does not reveal all the intricate features of the solutions. We estimate that a large amount of work still has to be done in the analysis of multirogue wave solutions.

To derive expressions for compound rogue waves and visualize them, there are currently two main procedures in favor: a method based on Wronskian determinants developed by Matveev's group [15,17–20], which has seen success in reaching the sixth order solution analytically [21], and the Darboux method [22–24], which we employ in this investigation. Most attempts thus far have assumed the free parameters in the solution to be zeros. In this case, all components of the higher order structure are aligned perfectly at one point and the field has a single high maximum. However, here, we deviate from this assumption. This has already been done to a limited extent and has produced the "rogue triplet" solution [15,20,25]. In this work, we extend this investigation to higher order solutions using both symbolic computation and numerics, and present surprising clustered structures reminiscent of an atom with a shell of electrons. Perfect geometrical patterns obtained here clearly demonstrate that the world of NLSE solutions is significantly richer than we thought before.

We begin by writing the NLSE in the dimensionless form,

$$i\frac{\partial\psi}{\partial x}+\frac{1}{2}\frac{\partial^2\psi}{\partial t^2}+|\psi|^2\psi=0. \tag{1}$$

The wave function $|\psi(x,t)|$ in Eq. (1) commonly describes the wave envelope. In fiber optic applications [11], the variable x is the distance along the fiber, while t is the retarded time in the frame moving with the pulse group velocity. On the other hand, in water wave applications [12], x is the dimensionless time, while t is the distance in the frame moving with the group velocity. This difference is related to conventions and traditions in each field, rather than to any particular physical meaning. A simple linear transformation with the variable involving the group velocity allows us to change the equation and variables from one form to another. Generally speaking, the linear relation between the two variables in this transformation may be one of the essential points for understanding the unusual results of our work; namely, the high level of symmetry in the (x,t) plane.

There is a class of first order solutions to Eq. (1) that can be described by a complex eigenvalue l with imaginary part $\mathrm{Im}(l)$. This whole class has been previously presented [26]. If $0<\mathrm{Im}(l)<1$, the solutions are periodic in t and localized in x. They are presently known as Akhmediev breathers (ABs) [27–30]. An example is shown in Fig. 1(a). If $\mathrm{Im}(l)>1$, the solution is localized in t and periodic in x. The solution is known as a Ma soliton. It is shown in Fig. 1(b). In the limit of $l\to i$, the period in both x and t goes to infinity and a solution involving rational terms arises. This first order wave function is known as the Peregrine soliton [9]. Due to localization both in space and time we can also call it a "wave that appears from nowhere and disappears without a trace" (WANDT) [13].

First order solutions are the simplest amidst NLSE solutions. Among more complicated known examples we can mention multisoliton solutions [23]. Via similar processes to the construction of this class, we can generate a nonlinear superposition of multi-AB solutions. This can be done in various ways, such as by following Wronskian methodology [17,18]. In this work, we employ an alternative procedure that uses Darboux transformations [31]. This allows for the nonlinear superposition of n ABs, each centered at an arbitrary coordinate (x_j,t_j) and each with a different eigenvalue l_j,

*djk105@rsphysse.anu.edu.au

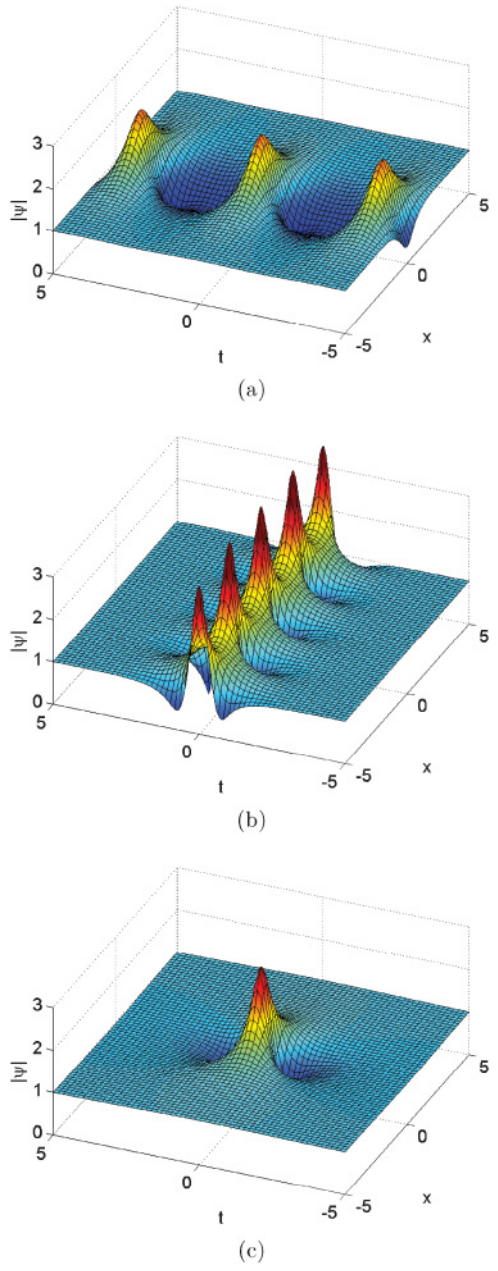

FIG. 1. (Color online) Various types of NLSE solution with l as eigenvalue. (a) Akhmediev breather with $l = 0.65i$. (b) Ma soliton with $l = 1.35i$. (c) Peregrine soliton with $l = i$ (or $\kappa = 0$).

where $j = 1,\ldots,n$. Frequencies of modulation are expressed through the eigenvalues as $\kappa_j = 2\sqrt{1+l_j^2}$. For AB solutions, these are real.

II. LOW ORDER ANALYTIC SOLUTIONS

The Darboux method [31] allows us to present exact solutions of any order explicitly. The process is described in the Appendix and elaborated elsewhere [24,32]. However, generally the method does not allow two AB components to share the same eigenvalue, otherwise degenerate solutions arise. In these situations, numerical simulations can also experience difficulties. One of the ways to overcome such obstacles is by defining the n eigenvalues in the form $\kappa_j = j\kappa$ $(j = 1,2,\ldots,n)$ and taking the limit $\kappa \to 0$ afterwards. The sequence of calculations has previously been described in detail [32,33] and will not be repeated here. The rational solution of order n in general form, depending on x and t, can be written as

$$\psi_n(x,t) = \left[(-1)^n + \frac{G_n + i\,H_n}{D_n}\right] e^{ix}, \tag{2}$$

where G_n, H_n, and D_n are all real polynomials of x and t.

A nontrivial observation is that higher order rational solutions are nonlinear combinations of the elementary component in Fig. 1(c). Their relative locations are uniquely defined by the shifts x_j and t_j, which effectively serve as coordinates of origin for each component. Depending on these parameters, we can have a variety of solutions of the same order n. A further nontrivial fact is that these shifts are eigenvalue dependent and need to be considered as functions of κ;

$$\begin{aligned} x_j &= \sum_{m=1}^{\infty} \kappa^{2(m-1)} X_{jm} \\ &= X_{j1} + X_{j2}\kappa^2 + X_{j3}\kappa^4 + \cdots, \\ t_j &= \sum_{m=1}^{\infty} \kappa^{2(m-1)} T_{jm} \\ &= T_{j1} + T_{j2}\kappa^2 + T_{j3}\kappa^4 + \cdots, \end{aligned} \tag{3}$$

where $1 \leqslant j \leqslant n$. The conceptual subtlety here is that, although the terms with nonzero orders of κ in Eq. (3) vanish in the $\kappa \to 0$ limit, analysis and numerics prove that their coefficients X and T have a crucial effect in defining the structure of higher order solutions.

In the first order case, $n = 1$, only X_{11} and T_{11} have any effect on the structure of the wave function in the $\kappa \to 0$ limit. So, for this $(n = 1)$ solution (Peregrine soliton), we have

$$\begin{aligned} G_1 &= 4, \\ H_1 &= 8(x - X_{11}), \\ D_1 &= 1 + 4(x - X_{11})^2 + 4(t - T_{11})^2. \end{aligned} \tag{4}$$

All higher order terms in Eq. (3) can be ignored. These two constants describe a simple translation of the solution in Fig. 1(c) relative to the origin. On the other hand, simple analytic study shows that the second order rational solution must have $X_{11} = X_{21}$ and $T_{11} = T_{21}$. Otherwise $\psi_2 \to \psi_0 = e^{ix}$ in the limit $\kappa \to 0$. Thus because such a requirement only involves a global shift of origin for all components, we can set $X_{j1} = T_{j1} = 0$ without loss of generality. Analytically, applying the $\kappa \to 0$ limit now produces the general second order $(n = 2)$ solution, described by

$$\begin{aligned} G_2 &= -\tfrac{1}{8}(5x^2 + t^2)(x^2 + t^2) - \tfrac{3}{16}(3x^2 + t^2) \\ &\quad + x x_d + t t_d + \tfrac{3}{128}, \\ H_2 &= -\frac{1}{4}x(x^2 + t^2)^2 - \frac{1}{8}x(x^2 - 3t^2) + \frac{15}{64}x \\ &\quad + \left(x^2 - t^2 - \frac{1}{4}\right) x_d + 2xtt_d, \end{aligned}$$

$$D_2 = \frac{1}{24}(x^2+t^2)^3 + \frac{1}{32}(3x^2-t^2)^2 + \frac{3}{128}(11x^2+3t^2) + \frac{3}{512} - \left(\frac{1}{3}x^3 - xt^2 + \frac{3}{4}x - \frac{2}{3}x_d\right)x_d - \left(x^2t - \frac{1}{3}t^3 + \frac{1}{4}t - \frac{2}{3}t_d\right)t_d, \quad (5)$$

where second order relative shifts are defined by the κ^2 coefficients of $x_1 - x_2$ and $t_1 - t_2$. Specifically

$$x_d = X_{12} - X_{22}, \qquad t_d = T_{12} - T_{22}. \quad (6)$$

When the relative shifts (x_d and t_d) between the components are zero, the resulting solution is an already known [13,33] second order rational solution with a single high maximum at the origin, shown in Fig. 2(a). When x_d and t_d are not zero, the second order peak breaks apart and, for sufficiently large second order shifts, forms a set of three first order rational solutions, the centers of which form an equilateral triangle. This solution is shown in Fig. 2(b). We have studied this

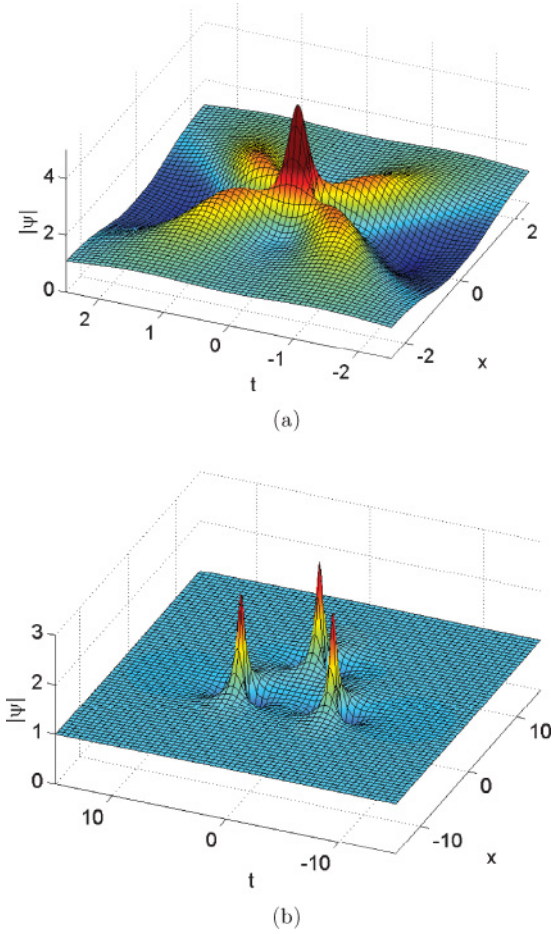

FIG. 2. (Color online) (a) Second order rational solution with zero shifts: $x_d = 0$ and $t_d = 0$. (b) Second order "rogue wave triplet" appears when $x_d = 5^2$ and $t_d = 0$.

form in detail [25] and can express the radius of the triangle's circumcircle in terms of x_d and t_d:

$$R \approx 2^{2/3}\left(x_d^2 + t_d^2\right)^{1/6}. \quad (7)$$

For the sake of comparison, we can relate the parameters γ and β found via the Wronskian methodology [18] with those of the current formalism by $\gamma = 2^5 x_d$ and $\beta = -2^5 t_d$.

As mentioned, analytically deriving general expressions for higher order rational solutions using the Darboux method is tedious, either by hand or with a computer. The Wronskian method appears to have had greater success generating these solutions [18,21]. However, incorporating the relative shift parameters this way is still difficult and has not been done.

III. HIGHER ORDER NUMERICAL RESULTS

Being a set of algebraic equations, the Darboux method can easily be converted into a numerical recursion procedure for any finite order n with eigenvalues and shifts as free adjustable parameters. It allows higher order rational solutions to be visualized in the $\kappa \to 0$ limit without presenting the cumbersome analytic expressions. Algebraic transformations can be done with high numerical accuracy to make the results indistinguishable from the rational solution. In fact, writing down the exact solutions would require many journal pages [18,21] and cannot be considered as a convenient way of presenting them.

In Fig. 3, we present higher order rational solutions, each with a single maximum at the origin, for $n = 3,4,5,6$. Analytical expressions for some of them have been presented earlier [14,21]. The maximum height of an order n rational solution is $2n+1$ and the structure also has $n(n+1)/2 - 1$ local maxima on each side of the $x = 0$ line. Starting from large negative x, an observer of its evolution would witness a row of n small peaks, then a row of $n-1$ larger peaks, then $n-2$ peaks, etc., before the central high amplitude solitary wave appears. The process is then symmetrically reversed in x so that, at large x, the wave "disappears without a trace." Thus, as noted before [21], the number of local maxima for an order n WANDT is $n(n+1) - 1$. For example, from Fig. 3(b) ($n = 4$), we see that successive rows have four, three, two, one, two, three, and finally four peaks.

Naturally, applying shifts changes the profiles. As was analytically evident with orders $n = 1$ and 2, it is also clear from numerics that only one coefficient per AB component from Eq. (3) has any effect on a higher order solution in the $\kappa \to 0$ limit; namely X_{jn} or T_{jn}, where j is the component number and n is the order of the solution. Here, we limit ourselves to shifting only one of the components; specifically, we apply the x shift in Eq. (3) to the first ($\kappa_1 = \kappa$) component alone. In this case, the $n = 3$ structure is solely determined by the $X_{13}\kappa^4$ term, the $n = 4$ structure by $X_{14}\kappa^6$, and so on. In each case, the coefficients of lower order κ terms must be the same between all components, otherwise $\psi_n \to \psi_{n-2}$ in the $\kappa \to 0$ limit. As for the coefficients of higher order κ terms, they are irrelevant.

The resulting wave functions for orders $n = 3,4,5,6$ are shown in Fig. 4. Remarkably, all higher order solutions display a ring structure. We observe rings with five peaks in Fig. 4(a), seven peaks in Fig. 4(b), etc. All peaks within the ring are first order rational solutions, i.e., Peregrine solitons. Naturally, each individual first order rational solution is always oriented in the

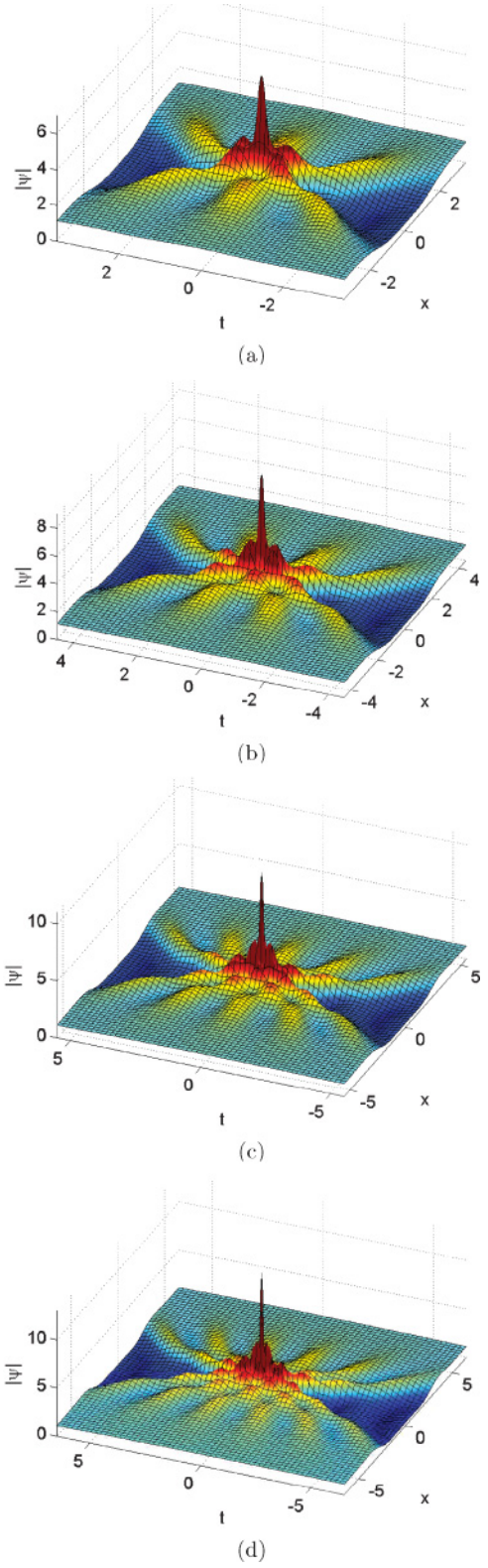

FIG. 3. (Color online) Higher order rational solutions with zero shifts, i.e., with its elementary components located at the origin. (a) The case of order $n = 3$. (b) $n = 4$. (c) $n = 5$. (d) $n = 6$.

same direction. Generally, the outer shell of an order n rational solution is composed of $2n - 1$ first order rational solutions. Evidently, the second order rogue wave triplet shown in Fig. 2(b) is the first in a series of higher order "shell" structures.

Another remarkable feature of these solutions is the presence of the central peak in each of them. Moreover, the central peak becomes more complicated with increasing n. When $n = 2$, the central peak is absent. When $n = 3$, the central peak is the same as the others, i.e., a first order rational solution. When $n = 4$, the central peak is more complicated. In fact, it is the $n = 2$ solution with zero shifts, i.e., the one shown in Fig. 2(a). All higher order solutions similarly display a central structure, which in each case is the order $n - 2$ rational solution with zero shifts. For example, the fifth order rational solution in Fig. 4(c) has a third order WANDT remaining in the middle of the structure. Likewise, after applying a shift proportional to κ^{10}, the sixth order rational solution shown in Fig. 4(d) has a fourth order rational solution in the middle. Generally, any sufficiently large shift moves $2n - 1$ first order rational solutions to its outer circular shell, leaving in the middle a WANDT of order $n - 2$.

Based on numerical evidence, we conjecture that the radius of the shell in the (x,t) plane for higher order structures follows a similar relation to Eq. (7), viz.

$$R \propto \left(X_{1n}^2 + T_{1n}^2\right)^{1/[2(2n-1)]}. \tag{8}$$

However, confirmation of a proportionality constant will require analytic expressions for the higher order wave functions. Furthermore, as the number of component shifts x_j that we can take to be nonzero is increased with n, additional relative shifts may split the central structure and create more shells.

IV. DISCUSSION: ROGUE WAVE "ATOMS"

Comparing our results with those of Matveev's group [15,17–20], published recently, our main achievements are as follows:

(1) We have found the relation between the shift parameters of the Darboux transformation scheme and the free parameters of the multirogue wave solutions that control their structure. These relations are important and far from being trivial.

(2) We have revealed the highly symmetric structure of multirogue wave solutions in the (x,t) plane. This is also a highly nontrivial result, as plotting the solutions does not reveal the symmetry immediately [15,17–20].

(3) We have found that, when we change their free parameters, the multirogue wave solutions split into substructures.

One way to interpret the wave functions in Fig. 4 is as atomic structures in the (x,t) plane with a "nucleus" and "electrons." Presently, this analogy is nothing other than visual. First, atoms are located in real space rather than in the (x,t) plane, unlike rogue waves of the NLSE. Second, real atoms with several shells are significantly more complicated. Thus this analogy still needs careful consideration, which may show that there is no real basis for it. Nevertheless, we cannot reject this attractive idea from the very beginning.

In order to see more similarities beyond the visual one, we note that, in a real atom, the first subshell s can have two electrons and each subsequent subshell has four more electrons than the previous subshell. Thus subshells p,d,f,g can have maxima of $6,10,14,18$ electrons, respectively. So the nth full shell has $2 + 6 + \cdots + (4n - 2) = 2n^2$ electrons. Likewise, an order n rogue wave for even n has an increasing number of electrons in the shells. If the core of the rogue wave

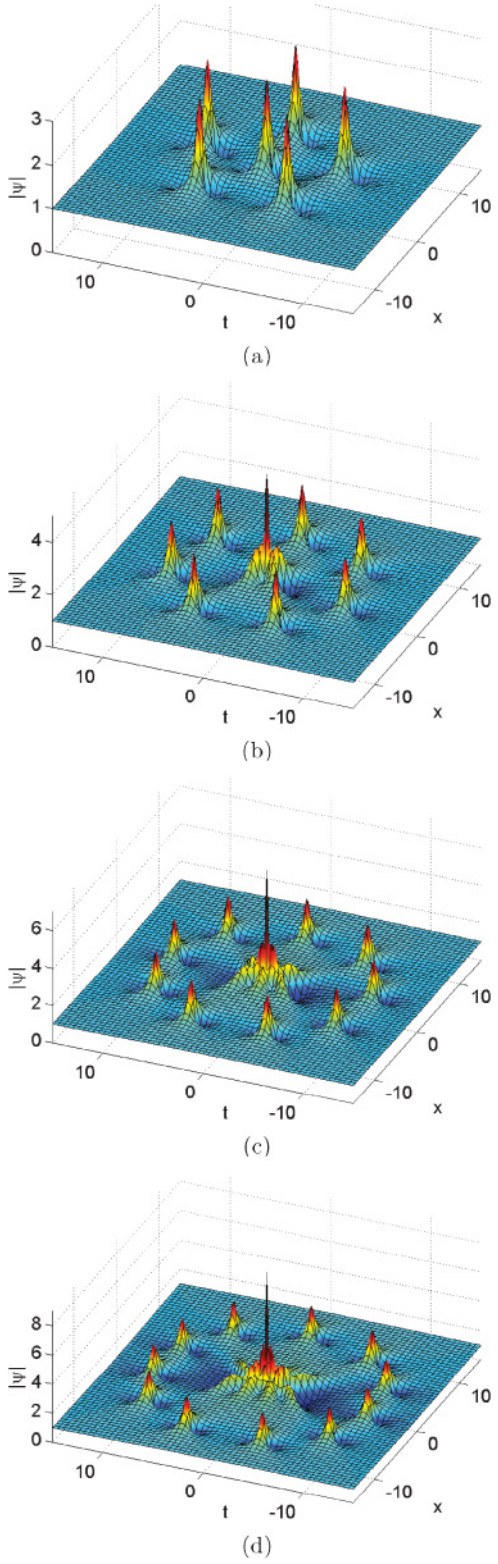

FIG. 4. (Color online) Higher order WANDTs with only the first component shifted. All $X_{1k} = 0$ unless specified. (a) Order 3 with $X_{13} = 5^4$. (b) Order 4 with $X_{14} = 5^6$. (c) Order 5 with $X_{15} = 5^8$. (d) Order 6 with $X_{16} = 5^{10}$.

cluster were to be expanded into several rings, it would be evident that the series in this case is $3 + 7 + \cdots + (2n - 1)$ with the total number of electrons being $n(n + 1)/2$. Similarly, for odd n the sum is $1 + 5 + \cdots + (2n - 1) = n(n + 1)/2$. Furthermore, the nature of this electron series is likely related to the denominator of the polynomial expression for the nth rogue wave, which is of order $n(n + 1)$ [14].

Curiously, there may also be some link with the nuclear shell model in that, if nuclear levels are labeled as $n = 1,2,3, \ldots$, then the number of states in level n is also $n(n + 1)$. Thus the analogies may actually be more profound than at first consideration. Further study may explain why the NLSE rogue wave cluster arranges itself in a regular fashion reminiscent of atomic shell theory.

With regard to experiment, a major application of these results might be found in optics or with deep water waves. Indeed, the simplest of these structures, namely the Peregrine soliton, has been recently observed in each of these cases [11,12]. These experiments clearly demonstrated that rogue wave solutions do exist and, moreover, the governing equation for these waves is indeed the NLSE. Using more complicated initial conditions in the corresponding experiments may lead to the observation of higher order structures described in the present work. Such experiments would confirm to what extent we can use the NLSE as a model for these waves. There is already no doubt that rogue wave triplets could be observed with ease as they essentially consist of three separated Peregrine solitons. For structures of higher order, such observations are more difficult but certainly worthy of trial. Taking into account that the new solutions are highly nontrivial, experiments will require significant effort to upgrade the capability of both controlled rogue wave production and detection. Nonetheless, we suggest that a progressive experimental program could feasibly generate circular rogue wave clusters within the next few years.

In some physical applications, e.g., optical self-focusing, both variables are spatial. In such a case, the whole geometric structure appears in two-dimensional space. On the other hand, in problems related to wave propagation, the time and space variables are related through the group velocity and can be swapped. Thus we can see these solutions either in a (t,t) or (x,x) plane. Perhaps this is a clearer way of understanding the beauty of the geometric structure of these formations.

In conclusion, we have studied families of higher order rational solutions of the NLSE with free real parameters. We have shown that these parameters are responsible for the "diffusion" of the central peak of the solution into clusters with a high level of symmetry. The clusters are arranged in circular shells, similar to the structure of electron shells in atoms.

ACKNOWLEDGMENTS

The authors acknowledge the support of the Australian Research Council (Discovery Project No. DP110102068). N.A. and A.A. acknowledge the support from the Volkswagen Stiftung. N.A. acknowledges support from the Alexander von Humboldt Foundation.

APPENDIX: THE DARBOUX METHOD

The NLSE arises from the compatibility of the following linear equations:

$$\frac{\partial R}{\partial t} = lJR + UR, \quad \frac{\partial R}{\partial x} = l^2 JR + lUR + \frac{1}{2}VR, \qquad \text{(A1)}$$

with matrices

$$U = \begin{pmatrix} 0 & i\psi^* \\ i\psi & 0 \end{pmatrix}, \quad V = \begin{pmatrix} -i|\psi|^2 & \frac{\partial \psi}{\partial t}^* \\ -\frac{\partial \psi}{\partial t} & i|\psi|^2 \end{pmatrix},$$
$$J = \begin{pmatrix} i & 0 \\ 0 & -i \end{pmatrix}, \quad R = \begin{pmatrix} r \\ s \end{pmatrix}, \tag{A2}$$

and l as a complex eigenvalue.

Choosing a seeding solution of

$$\psi_0 = e^{ix} \tag{A3}$$

and restricting l to being purely imaginary, the system in Eq. (A1) is compatible with $\psi = \psi_0$ when $r = r_{1j}$ and $s = s_{1j}$, defined as

$$r_{1j} = 2ie^{-ix/2}\sin(A_{jr} + iA_{ji}),$$
$$s_{1j} = 2e^{ix/2}\cos(B_{jr} + iB_{ji}). \tag{A4}$$

The subscripts r and i refer to real and imaginary parts, respectively. The functions A and B are then given by

$$A_{jr} = \frac{1}{2}\left[\arccos\left(\frac{\kappa_j}{2}\right) + (t - t_j)\kappa_j - \frac{\pi}{2}\right],$$
$$B_{jr} = \frac{1}{2}\left[-\arccos\left(\frac{\kappa_j}{2}\right) + (t - t_j)\kappa_j - \frac{\pi}{2}\right],$$
$$A_{ji} = B_{ji} = \frac{1}{2}\left[(x - x_j)\kappa_j\sqrt{1 - \frac{\kappa_j^2}{4}}\right], \tag{A5}$$

where $\kappa_j = 2\sqrt{1 + l_j^2}$. The j subscript indicates that eigenvalue l_j and coordinate shifts (x_j, t_j) are free parameters. For example, $j = 4$ refers to the fourth set of eigenvalue and shift parameters.

A first order solution to the system in Eq. (A1) incorporates only one chosen set of free parameters and its corresponding r and s equations from Eq. (A4), denoted by $j = 1$. The first order wave function is thus expressed as

$$\psi_1 = \psi_0 + \frac{2(l_1^* - l_1)s_{11}r_{11}^*}{|r_{11}|^2 + |s_{11}|^2}. \tag{A6}$$

An order $n > 1$ solution requires higher order versions of the expressions for r and s. These are recursively generated [24,32] by

$$\begin{aligned} r_{np} = {} & [(l_{n-1}^* - l_{n-1})s_{n-1,1}^* r_{n-1,1}s_{n-1,p+1} \\ & + (l_{p+n-1} - l_{n-1})|r_{n-1,1}|^2 r_{n-1,p+1} \\ & + (l_{p+n-1} - l_{n-1}^*)|s_{n-1,1}|^2 r_{n-1,p+1}] \\ & /(|r_{n-1,1}|^2 + |s_{n-1,1}|^2), \\ s_{np} = {} & [(l_{n-1}^* - l_{n-1})s_{n-1,1}r_{n-1,1}^* r_{n-1,p+1} \\ & + (l_{p+n-1} - l_{n-1})|s_{n-1,1}|^2 s_{n-1,p+1} \\ & + (l_{p+n-1} - l_{n-1}^*)|r_{n-1,1}|^2 s_{n-1,p+1}] \\ & /(|r_{n-1,1}|^2 + |s_{n-1,1}|^2). \end{aligned} \tag{A7}$$

The p subscript in Eq. (A7) is used purely for enumeration and does not necessarily refer to a particular set of parameters. For example, the second order function r_{21} involves the first order sets r_{11}, s_{11}, r_{12}, and s_{12}. Similarly, the third order function r_{31} involves the second order functions r_{21}, s_{21}, r_{22}, and s_{22}, which, in turn, are based on r_{11}, s_{11}, r_{12}, s_{12}, r_{13}, and s_{13} at the lowest order of recursion. This way, Eq. (A7) allows n sets of free parameters to be incorporated into an order n solution. The diagram in Fig. 2.2 of the *Solitons* book [32] can be of use in representing this sequence of calculations. Then, the order n NLSE solution is generated through recursion by

$$\psi_n = \psi_{n-1} + \frac{2(l_n^* - l_n)s_{n1}r_{n1}^*}{|r_{n1}|^2 + |s_{n1}|^2}. \tag{A8}$$

In this work we are mainly interested in the specific case of the $\kappa_j \to 0$ limit. Then all unequal κ_j are expressed in terms of a common variable such as κ. The numerator and denominator from every iteration of Eq. (A8) is then Taylor expanded in terms of κ and only the lowest order is retained. This results in "rational" solutions, such as Eqs. (4) and (5).

[1] A. R. Osborne, *Nonlinear Ocean Waves And The Inverse Scattering Transform* (Academic Press, New York, 2010).
[2] E. Pelinovsky and C. Kharif, *Extreme Ocean Waves* (Springer, Berlin, Heidelberg, 2008).
[3] C. Garrett and J. Gemmrich, Phys. Today **62**(6), 62 (2009).
[4] D. R. Solli, C. Ropers, P. Koonath, and B. Jalali, Nature (London) **450**, 1054 (2007).
[5] M. Shats, H. Punzmann, and H. Xia, Phys. Rev. Lett. **104**, 104503 (2010).
[6] V. B. Efimov, A. N. Ganshin, G. Kolmakov, P. McClintock, and L. Mezhov-Deglin, Eur. Phys. J. Spec. Top. **185**, 181 (2010).
[7] Y. V. Bludov, V. V. Konotop, and N. Akhmediev, Phys. Rev. A **80**, 033610 (2009).
[8] F. T. Arecchi, U. Bortolozzo, A. Montina, and S. Residori, Phys. Rev. Lett. **106**, 153901 (2011).
[9] D. Peregrine, J. Aust. Math. Soc. Series B **25**, 16 (1983).
[10] V. Shrira and V. Geogjaev, J. Eng. Math. **67**, 11 (2010).
[11] B. Kibler, J. Fatome, C. Finot, G. Millot, F. Dias, G. Genty, N. Akhmediev, and J. M. Dudley, Nat. Phys. **6**, 790 (2010).
[12] A. Chabchoub, N. P. Hoffmann, and N. Akhmediev, Phys. Rev. Lett. **106**, 204502 (2011).
[13] N. Akhmediev, A. Ankiewicz, and M. Taki, Phys. Lett. A **373**, 675 (2009).
[14] N. Akhmediev, A. Ankiewicz, and J. M. Soto-Crespo, Phys. Rev. E **80**, 026601 (2009).
[15] P. Dubard, P. Gaillard, C. Klein, and V. Matveev, Eur. Phys. J. Spec. Top. **185**, 247 (2010).
[16] A. Ankiewicz, P. Clarkson, and N. Akhmediev, J. Phys. A **43**, 122002 (2010).
[17] P. Gaillard, preprint: halshs-00536287, version 1 - 15 Nov. 2010.
[18] P. Gaillard, preprint: hal-00573955, version 2 - 7 Apr. 2011.
[19] P. Gaillard, J. Phys. A **44**, 435204 (2011).
[20] P. Dubard and V. B. Matveev, Nat. Hazards Earth Syst. Sci. **11**, 667 (2011).

[21] P. Gaillard, preprint: hal-00589556, version 1 - 29 Apr. 2011.
[22] V. B. Matveev and M. Salle, *Darboux Transformations and Solitons* (Springer-Verlag, Berlin, Heidelberg, 1991).
[23] N. Akhmediev and N. V. Mitskevich, IEEE J. Quantum Electron. **27**, 849 (1991).
[24] N. Akhmediev, J. M. Soto-Crespo, and A. Ankiewicz, Phys. Lett. A **373**, 2137 (2009).
[25] A. Ankiewicz, D. J. Kedziora, and N. Akhmediev, Phys. Lett. A **375**, 2782 (2011).
[26] N. Akhmediev, V. M. Eleonskii, and N. E. Kulagin, Teor. Math. Fiz. (USSR) **72**, 183 (1987) [Theor. Math. Phys. **72**, 809 (1988)].
[27] K. B. Dysthe and K. Trulsen, Phys. Scr. **T82**, 48 (1999).
[28] I. Ten and H. Tomita, Reports of RIAM Symposium No. 17SP1-2, Chikushi Campus, Kyushu University, Kasuga, Fukuoka, Japan, March 10–11, 2006.
[29] D. Clamond, M. Francius, J. Grue, and C. Kharif, Eur. J. Mech. B **25**, 536 (2006).
[30] V. V. Voronovich, V. I. Shrira, and G. Thomas, J. Fluid Mech. **604**, 263 (2008).
[31] N. Akhmediev, V. I. Korneev, and N. V. Mitskevich, Zh. Eksp. Teor. Fiz. **94**, 159 (1988) [Sov. Phys. JETP **67**, 89 (1988)].
[32] N. Akhmediev and A. Ankiewicz, *Solitons: Nonlinear Pulses and Beams*, Optical and Quantum Electronics Vol. 5 (Chapman & Hall, London, 1997), Chaps. 3 and 4.
[33] N. Akhmediev, V. M. Eleonskii, and N. E. Kulagin, Zh. Eksp. Teor. Fiz. **89**, 1542 (1985) [Sov. Phys. JETP **62**, 894 (1985)].